

The enigmatic He-sdB pulsator LS IV-14°116 : new insights from the VLT[★]

S.K. Randall¹, S. Bagnulo², E. Ziegerer³, S. Geier¹, and G. Fontaine⁴

¹ ESO, Karl-Schwarzschild-Str. 2, 85748 Garching bei München, Germany; e-mail: srandall@eso.org

² Armagh Observatory, College Hill, Armagh BT61 9DG, Northern Ireland, UK

³ Dr. Remeis-Observatory & ECAP, Astronomical Institute, Friedrich-Alexander University Erlangen-Nürnberg, Sternwartstr. 7, 96049 Bamberg, Germany

⁴ Département de Physique, Université de Montréal, C.P. 6128, Succ. Centre-Ville, Montréal, QC H3C 3J7, Canada

Received date / Accepted date

ABSTRACT

The intermediate Helium subdwarf B star LS IV-14°116 is a unique object showing extremely peculiar atmospheric abundances as well as long-period pulsations that cannot be explained in terms of the usual opacity mechanism. One hypothesis invoked was that a strong magnetic field may be responsible. We discredit this possibility on the basis of FORS2 spectro-polarimetry, which allows us to rule out a mean longitudinal magnetic field down to 300 G.

Using the same data, we derive the atmospheric parameters for LS IV-14°116 to be $T_{\text{eff}} = 35,150 \pm 111$ K, $\log g = 5.88 \pm 0.02$ and $\log N(\text{He})/N(\text{H}) = -0.62 \pm 0.01$. The high surface gravity in particular is at odds with the theory that LS IV-14°116 has not yet settled onto the Helium Main Sequence, and that the pulsations are excited by an ϵ mechanism acting on the Helium-burning shells present after the main Helium flash.

Archival UVES spectroscopy reveals LS IV-14°116 to have a radial velocity of 149.1 ± 2.1 km/s. Running a full kinematic analysis, we find that it is on a retrograde orbit around the Galactic centre, with a Galactic radial velocity component $U = 13.23 \pm 8.28$ km/s and a Galactic rotational velocity component $V = -55.56 \pm 22.13$ km/s. This implies that LS IV-14°116 belongs to the halo population, an intriguing discovery.

Key words. Stars: individual: LS IV-14°116 — Stars: subdwarfs — Stars: magnetic field — Stars: kinematics and dynamics — Stars: atmospheres — Stars: oscillations — Stars: chemically peculiar

1. Introduction

Pulsating subdwarf B (sdB) stars have received a lot of attention over the last years. Having become one of the success stories of asteroseismology, they hold the key to a more mature understanding of the formation and evolution of hot subdwarfs. While it is commonly accepted that sdB stars are compact, evolved, He-core burning objects that lost too much of their H-envelope before or at the He-flash to sustain H-shell burning, the details of their evolution and in particular the mass loss mechanism remain unclear. A large fraction of field subdwarf B stars are found to reside in binary systems and may have been stripped of their envelope mass by binary interactions involving Roche lobe overflow and/or a common envelope phase (Han et al. 2002, 2003), potentially resulting in a late Helium-flash (e.g., Brown et al. 2001). Single sdB stars have been explained by mergers involving at least one white dwarf (Han 2008; Clausen & Wade 2011) or a Helium-enriched subpopulation in Globular Clusters (e.g., D’Antona et al. 2005).

First discovered in the late nineties (Kilkenny et al. 1997), the rapidly pulsating sdB stars show luminosity variations on timescales of 100–200 s and are found in a well-defined instability strip between $\sim 29,000$ – $36,000$ K. The fast pulsations have been modelled very successfully in terms of pressure (p)-mode instabilities excited by an opacity (κ)-mechanism associ-

ated with a local overabundance of iron in the driving region (Charpinet et al. 1996, 1997). While sdB stars are overall metal-poor, diffusion (the competitive action between radiative levitation and gravitational settling) creates a non-uniform abundance profile of heavy elements as a function of depth. As a consequence, all sdB stars observed so far show chemically peculiar atmospheric abundances, and the vast majority of them ($\sim 90\%$) are Helium-deficient (ranging from no detected Helium to nearly Solar). Diffusion is also the key ingredient to understanding the pulsation driving in a well-defined instability strip in surface gravity - effective temperature ($\log g - T_{\text{eff}}$) space: depending on the exact balance between the levitation of heavy elements caused by the radiation pressure (dependent on T_{eff}) and the gravitational settling (dependent on $\log g$) an iron-“bump” is formed, causing a sharp peak in opacity at the right depth to drive pulsations, or not. The depth at which pulsations are excited depends critically on their type: the rapid p -mode pulsations are driven in the outer envelope regions, whereas in contrast the longer-period gravity modes (g -modes) are produced deeper inside the star. And indeed, the iron opacity mechanism also gives rise to a second type of sdB pulsator with longer ($P \sim 2000$ – 8000 s) g -mode pulsations, members of which are located in a cooler instability strip between $22,000$ – $29,000$ K (Green et al. 2003). It is then quite fitting that stars located at the intersection between the p - and g -mode instability regions appear to be hybrids and show both rapid and slow luminosity variations (Schuh et al. 2006). The two types of sdB pulsator have now been very successfully analyzed using asteroseismol-

[★] Based on observations collected at the European Organisation for Astronomical Research in the Southern Hemisphere, Chile (proposal ID 093.D-0680 and 087.D-0950)

ogy (e.g., Van Grootel et al. 2013; Charpinet et al. 2011), where the internal parameters of the star are derived from the observed pulsation spectrum to a high accuracy and can be used to start constraining the proposed evolutionary scenarios.

Given that the pulsation properties of the two types of sdB pulsator are so well defined, it was a surprise when long-period ($P \sim 2000\text{--}5000$ s), multi-periodic luminosity variations were detected in the hot ($T_{\text{eff}} \sim 35,000$ K) sdB star LS IV-14°116 (Ahmad & Jeffery 2005; Green et al. 2011). While exhibiting pulsation periods typical of the g -mode pulsators, this unique star is located right in the middle of the hotter p -mode instability strip (see Fig. 5 of Green et al. 2011), where the longer pulsations observed cannot be explained by the κ -mechanism. As an alternative, it was suggested that the observed pulsations may be excited by an ϵ -mechanism acting in the He-burning shells that appear before the star settles in the core He-burning stage (Miller Bertolami et al. 2011).

Compared to the other, H-rich sdB pulsators, LS IV-14°116 is also different in that it shows a mild atmospheric Helium-enhancement ($\log N(\text{He})/N(\text{H}) \sim -0.6$). This makes it an intermediate He-rich sdB, and as such a potential asteroseismic probe of a different evolutionary phase to the other sdB pulsators. For instance, it has been suggested that He-sdBs are the immediate progenitors of H-sdBs, before the Helium has had time to be depleted from the atmosphere due to gravitational settling (Jeffery 2012). Apart from being the only He-rich sdB pulsator, LS IV-14°116 also shows a very strange abundance pattern even for a subdwarf B star, with Ge, Sr, Y and Zr enhanced by factors of up to 10,000 compared to Solar (Naslim et al. 2011). One of the most plausible explanations invoked for these observed overabundances was radiative levitation in a particularly quiet atmosphere invoked by a strong (\gtrsim kG) magnetic field. Such a magnetic field would presumably affect the driving of pulsation modes, and potentially shift the g -mode instability strip to higher temperatures, thus naturally explaining the pulsations observed in LS IV-14°116.

The main aim of the study presented here was to check LS IV-14°116 for the presence of a magnetic field with a disk-averaged longitudinal component of a few hundred Gauss or higher using the spectro-polarimetric capability of FORS2 at the VLT on Cerro Paranal, Chile. This facility has over the last decade been used extensively to study stellar magnetism, and led to claims of magnetic field detections in a variety of stars across the Hertzsprung-Russell diagram, including hot subdwarfs (O’Toole et al. 2005). However, several of these detections (including those presented for sdB stars) were later shown to be artefacts of the data reduction procedure in a systematic analysis of FORS2 spectro-polarimetric archival data (Bagnulo et al. 2012; Landstreet et al. 2012a). An independent analysis based on spectro-polarimetry obtained with ESPaDOnS at the CFHT (Petit et al. 2012) also failed to measure a magnetic field in two hot subdwarfs for which a positive detection had previously been claimed. In this context, it was with great interest that we noted the first detection of a very strong (several hundred kG) magnetic field in a He-rich subdwarf O star (Heber et al. 2013). Given that magnetic fields are relatively common among white dwarfs, they should also be present for a sizeable fraction of their hot subdwarf (sdB and sdO) progenitors. With its puzzling pulsational properties and atmospheric abundance profile, LS IV-14°116 was then a prime candidate for the first magnetic sdB star.

In the following sections we present the FORS2 spectro-polarimetry gathered and the resulting null detection of a magnetic field. We then move on to the exploitation of the FORS2 total intensity spectra and supplement these with UVES archival

data to show that LS IV-14°116 is very likely a halo star. The paper ends with a discussion of the open questions regarding this unique object.

2. No evidence for a magnetic field

Our spectro-polarimetric data were gathered with FORS2/VLT in the second half of the night on 4th and 5th June 2014 in visitor mode, which allowed us to use the blue-sensitive E2V CCD. We chose the 1200B grism covering the $\sim 3600\text{--}5200$ Å range and a variable slit width of 1'' for June 4 and 0.7'' for June 5, yielding a nominal wavelength resolution of $\Delta\lambda \sim 3.1$ Å and 2.3 Å for the two nights respectively. The slit width was adjusted to limit slit losses due to the poor seeing (1.5-2'') on the first night and kept at the originally desired value on the second night (seeing of 0.8-1.2''). We employed a shutter time of 600 s per exposure and set up the observing sequence so as to alternate between two different retarder waveplate settings of -45° and $+45^\circ$. On the first night we obtained 16 exposures (8 at each of the retarder plate settings), while on the second night we managed to collect 30 spectra (15 pairs at perpendicular retarder plate settings). In total, we gathered nearly 8 hours of useful data on-target, the aim being to reach a $S/N \gtrsim 2000/\text{\AA}$ for this relatively faint ($B \sim 13.0$) target. We also observed the bright spectropolarimetric standard HD 94660 using the exact same instrument setup as a sanity check.

Data reduction was done closely following the procedure developed and described by Bagnulo et al. (2012). Simply put, we calculated two profiles: the circular polarisation normalised to the intensity $P_V = V/I$ (where V is the Stokes parameter measuring the circular polarization and I is the usual unpolarized intensity), and the null profile N_V , which is representative of the noise of P_V . We obtained the ‘rectified’ version of these quantities by combining the series of exposure pairs taken at perpendicular retarder waveplate settings using Eq. (3) of Bagnulo et al. (2012). The results are illustrated in Fig. 1 for the second night of observations (the result for the first night is qualitatively the same, but the S/N is lower). The top panel shows the total intensity (i.e. the time-averaged spectrum) together with P_V and N_V as a function of wavelength. Even more interesting are the diagnostic plots in the lower panels, as is explained in what follows. The maximum S/N in the spectrum is ~ 2500 per Å.

Under the so called “weak-field” approximation, the intensity of circular polarisation (due to the Zeeman effect) across a spectral line can be expressed as:

$$P_V = -g_{\text{eff}} C_z \lambda^2 \frac{1}{I} \frac{dI}{d\lambda} \langle B_z \rangle \quad (1)$$

where g_{eff} is the effective Landé factor, λ is the wavelength, C_z is a constant and $\langle B_z \rangle$ is the mean longitudinal magnetic field expressed in G. The longitudinal field is the integrated line-of-sight component of the magnetic field. As can be deduced from Eq. (1), the latter is obtained as the slope of a linear regression of V/I versus the quantity $-g_{\text{eff}} C_z \lambda^2 (1/I) dI/d\lambda$, which is precisely what is plotted in the bottom left-hand panel of Fig.1. Note that for the hydrogen lines of a star with $T_{\text{eff}} \sim 35,000$ K and a dipolar field, the “weak-field” approximation is formally valid for field strengths up to 10-20 kG (see, e.g. Eq. 1 from Bagnulo et al. 1995).

A visual inspection of P_V yields no evidence for the presence of a strong magnetic field. Using the least-squares technique discussed in Bagnulo et al. (2002) and applying it to all spectral

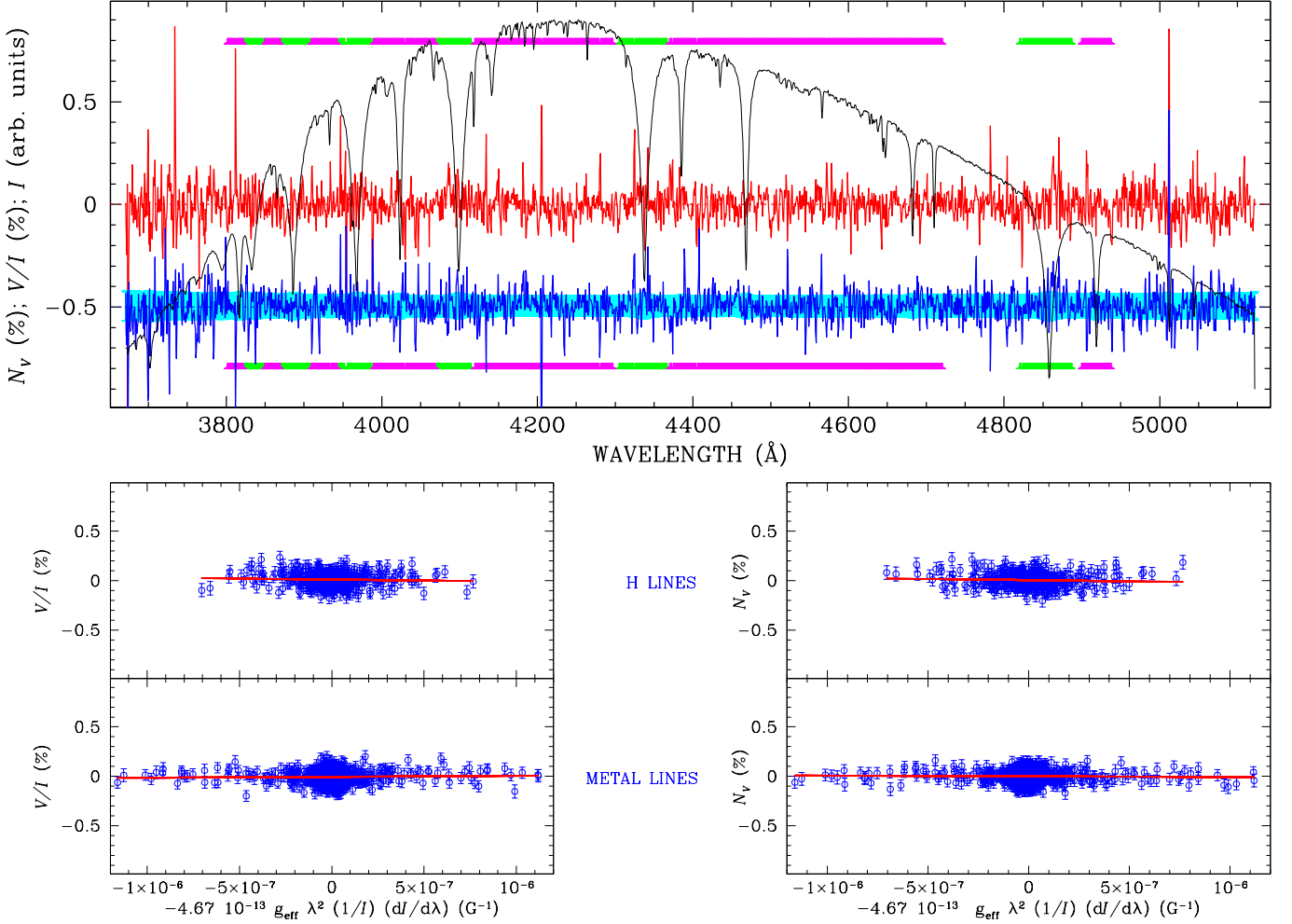


Fig. 1. *Top:* The total intensity FORS2 spectrum I (black) together with the normalised circular polarisation P_V (red) and the Null profile N_V (blue) obtained by combining all data taken on 2014-06-05 for LS IV-14°116. The null profile is offset by -0.5% for display purposes, the 1σ errors expected from photon noise being represented by the light blue error bars. The green (magenta) marked wavelength ranges indicate the portions of the spectrum used for the analysis based on the H (metal) lines respectively. *Bottom:* P_V (left) and N_V plotted as a function of the quantity indicated on the x-axis. The slope of P_V in this diagram is proportional to the mean longitudinal magnetic field $\langle B_z \rangle$. The plots refer to the results obtained from using the H lines (green portions of the wavelength range in the top plot) and the metal lines (magenta portions) as indicated.

lines we measure $\langle B_z \rangle = 9 \pm 93$ G, a null detection within the error bar of about 100 G. From the H lines alone we derive $\langle B_z \rangle = -180 \pm 205$ G and from the He and metal lines we find $\langle B_z \rangle = 97 \pm 105$. The observations obtained during the first night also resulted in a null detection, although with a larger uncertainty due to the smaller S/N ratio of the spectra. As expected, null detections were also obtained from the null profiles, confirming the reliability of our results. However, in Fig. 1 both the P_V and N_V profiles show more scatter around zero than would be expected from photon noise alone (i.e. the scatter in the profiles is larger than the light blue 1σ error bars). A deeper inspection of our data reveals that spectra obtained during an observing series are slightly offset from each other. If interpreted in terms of radial velocity, the observed shifts would suggest that during the observing series, the star has changed its radial velocity by about 40 km/s, which is probably unrealistic and most likely due to instrumental effects. We note that during the observing series the instrument rotated by about 120° while the airmass changed from

about 1.5 to 1.1. In these conditions, tests performed in imaging mode show that a differential shift of about 1 pixel is to be expected (see Fig. 2.4 of the FORS user manual); the presence of a grism and polarimetric optics will presumably strengthen this effect. We conclude that the observed shift is probably due to small instrument flexures, which in turns result in Stokes profiles noisier than expected from photon noise. For more detailed information see Bagnulo et al. (2013).

From the analysis above we claim a null detection of a magnetic field down to a 3σ threshold of 300 G. Note that, formally, this applies only to the mean longitudinal magnetic field (i.e. the magnetic field averaged over the visible disk in the direction of the line of sight) at the time of observation. The possibility remains that LS IV-14°116 in fact does have a strong dipolar field but that its longitudinal component was not detectable because we observed the magnetic field equator-on. Since a detailed analysis of the pulsation periods of LS IV-14°116 (Green et al. 2011) showed no indication of rotational splitting, we can assume that

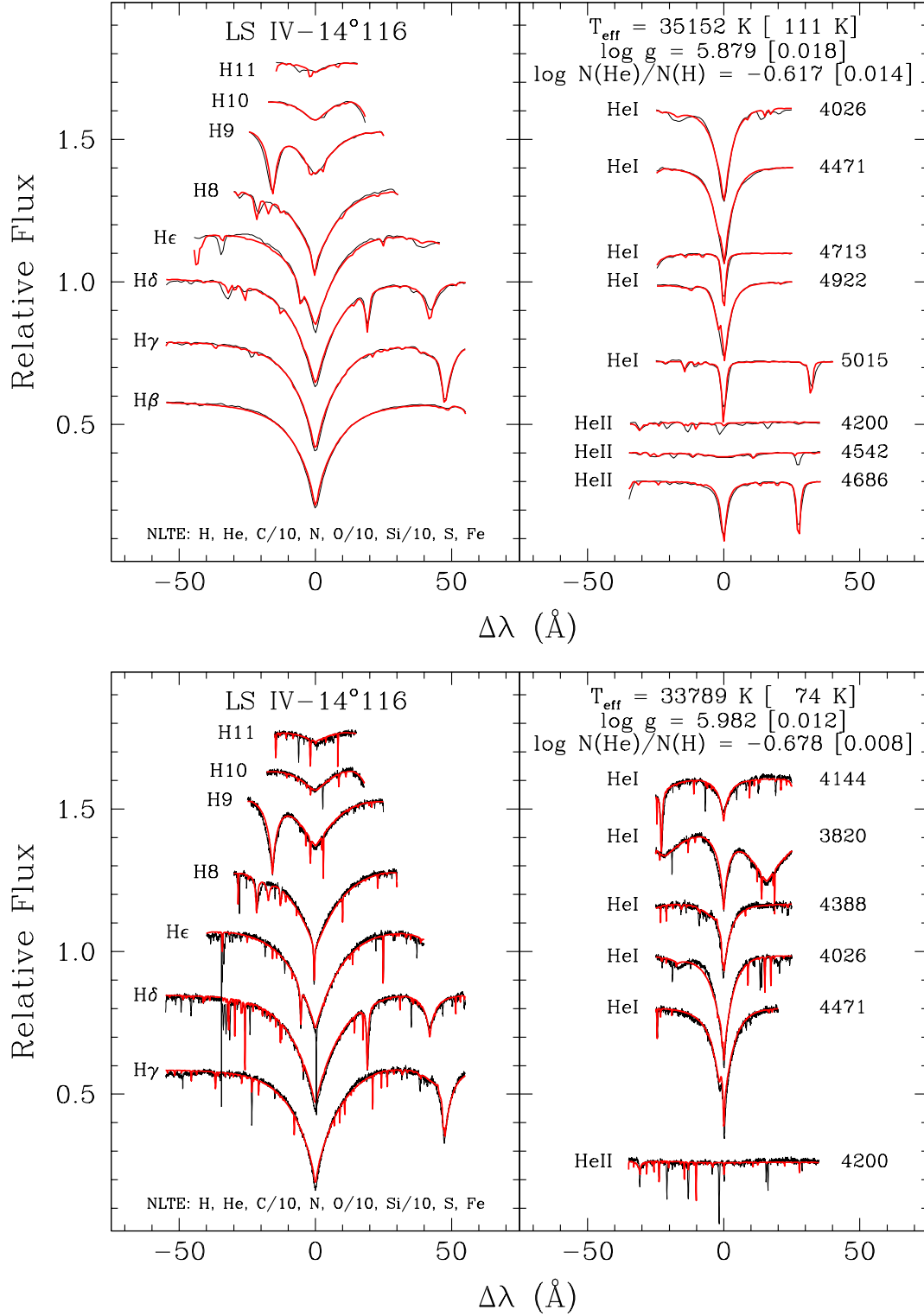


Fig. 2. *Left:* Fit to the Balmer and He lines in the FORS2 spectrum of LS IV-14°116. The thin black line is the observed spectrum and the thick red line represents the best-fit model atmosphere. The quoted uncertainties refer only to the formal fitting errors, and certainly underestimate the true errors. *Right:* The equivalent fit to the UVES spectrum.

our target is a slow rotator with a rotation period longer than a month or so. Therefore, our spectropolarimetric measurements over two consecutive nights would have been taken at a very similar rotational phase. Assuming a limb darkening coefficient of 1, the mean longitudinal field of a dipole is related to the field

strength at the magnetic pole B_p by

$$\langle B_z \rangle = 0.4 B_p \cos \ell \quad (2)$$

where ℓ is the angle of the dipolar axis with respect to the line of sight (see Eqs. 2 and 3 of Bagnulo et al. 1995). If we observed

the magnetic field pole-on we would then (at 3σ) have been sensitive to polar magnetic field strengths down to ~ 750 G, while at $\ell=45^\circ$ we would have barely detected a field with $B_p \sim 1$ kG. A dipole magnetic field with $B_p \gtrsim 5$ kG would then have had a 85% chance, one with $B_p \gtrsim 7.5$ kG a 90% chance of being detected from our measurements.

Another issue is that the technique used is sensitive mainly to the longitudinal component of a dipolar field. According to Eq. 5 of Landolfi et al. (1998), and again assuming a limb-darkening coefficient = 1, the contribution to the longitudinal field of any quadrupolar component is at best about six times smaller than the contribution due to the dipolar component. This implies that a quadrupolar field would have to be very strong indeed (at the 50 kG level or higher) to be detected by our measurements. According to the work of Mathys & Hubrig (2006) there is an empirical correlation between a dipole and a quadrupole magnetic field (which can be measured on the basis of line profiles) for roAp stars, i.e. stars with larger quadratic fields also have larger dipole fields. However, it is completely unclear whether such a correlation would hold for hot subdwarfs. The authors also point out that for a magnetic field to be detectable the organisation has to be large-scale enough for contributions of various parts of the stellar surface to not cancel out, and the geometry of the magnetic field along the line-of-sight has to be favourable.

The strong magnetic fields so far measured in white dwarfs tend to be dipole fields with strengths on the order of several MG, with weaker fields at the tens of kG level also having been detected in a small number of these stars (Landstreet et al. 2012b; Kawka & Vennes 2012). Similarly, the recently discovered magnetic He-sdO star (Heber et al. 2013) has a magnetic fields strong enough to induce clear Zeeman splitting (hundreds of kG). We would have been extremely unlucky to have missed anything remotely comparable to these in LS IV-14°116.

Our measurements for LS IV-14°116 can be contrasted with those we obtained for HD 94600, a bright Ap star with a well-measured magnetic field (e.g., Landstreet et al. 2014). Here, the exact same least-squares fitting technique yields an integrated line-of-sight magnetic field of $\langle B_z \rangle \sim -2200$ G. This is in line with predictions for the time of our observations (MJD~56813) assuming the candidate rotational period of the star of 2800 d (see Fig. 5 of Landstreet et al. 2014). Thus, the instrument setup and technique yielding the null detection reported above for LS IV-14°116 appear sound.

3. Spectroscopic analysis

While the main goal of the FORS2 observations proposed for LS IV-14°116 was the measurement of a possible magnetic field, the total intensity (Stokes I) spectra are also of interest. In particular, we planned to use the combined time-averaged spectrum obtained to determine the atmospheric parameters, and hoped to exploit the time-series of individual spectra for radial velocity (RV) measurements tracing the stellar pulsations. The latter study eventually proved fruitless due to the ~ 40 km/s RV drift over the course of the nightly observations discussed above. Attempts to correct for the instrumental drift yielded RV curves too noisy to detect pulsations at the expected few km/s level. Quite interestingly, we did note a strong absolute RV shift of around -150 km/s, which was either overlooked or dismissed as unimportant in previous studies of LS IV-14°116 (Ahmad & Jeffery 2005; Green et al. 2011; Naslim et al. 2011). We were able to confirm this blueshift from a re-analysis of high resolution UVES spectra downloaded from the ESO archive. The UVES dataset comprises a 4-hour time-series of around 30

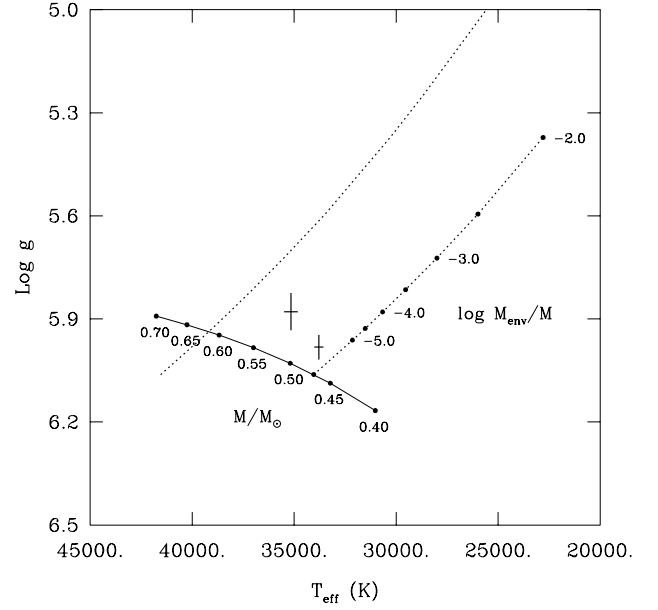


Fig. 3. We show the location of the Helium Main Sequence (solid line) in the $\log g - T_{\text{eff}}$ diagram for different stellar masses as indicated. The Zero-Age EHB (right-hand dotted line) and the Terminal-Age EHB (left-hand dotted line) are shown for different hydrogen envelope masses based on the Montréal 3rd generation evolutionary models. Superimposed on this is the location of LS IV-14°116 derived from the FORS2 (left) and UVES (right) spectra respectively. Both estimates place LS IV-14°116 firmly on the EHB; a star that has not yet settled on the EHB would be found at similar temperatures but significantly lower surface gravities (cf. Fig 1, Miller Bertolami et al. 2011).

spectra that were originally obtained with the aim of detecting pulsational radial velocity variations, and the details of this are published elsewhere (Jeffery et al. 2014, MNRAS, submitted). For the purposes of the present study, we focus exclusively on the time-averaged absolute radial velocities and the combined spectrum.

3.1. Atmospheric parameters

The atmospheric parameters so far derived for LS IV-14°116 by two independent groups (Naslim et al. 2011; Green et al. 2011) are somewhat at odds with each other, in particular as far as the surface gravity derived is concerned. On the basis of their high resolution echelle spectra, Naslim et al. (2011) measured $T_{\text{eff}}=34,500 \pm 500$ K and $\log g=5.6 \pm 0.2$, while Green et al. (2011) report $T_{\text{eff}}=34,950 \pm 250$ K and $\log g=5.93 \pm 0.04$. We made use of the combined spectrum from both our FORS total intensity spectra and the UVES archival data to re-evaluate the atmospheric parameters of LS IV-14°116.

The FORS2 combined spectrum was computed using our individual spectra obtained on June 5 only, i.e. those with the better spectral resolution of $\Delta\lambda \sim 2.3$ Å. This yielded a high quality time-averaged spectrum covering the 3650-5100 Å range, including the Balmer lines from H β upward as well as 8 strong Helium lines. These were fit using our standard grids of NLTE model atmospheres and synthetic spectra (see e.g. Brassard et al. 2010, for details) incorporating a fixed metallicity inspired by

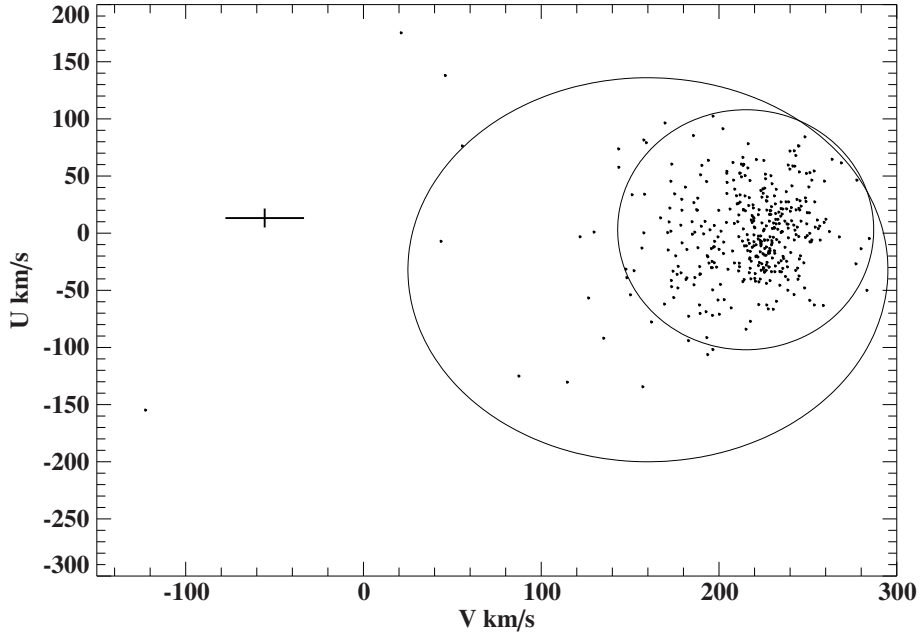


Fig. 4. U-V diagram showing the position of LS IV-14°116 (thick error bars) as compared to 3- σ thin disk and 3- σ thick disk contours. Stars located outside these contours have kinematic properties of the halo population. The points inside the contours correspond to the reference white dwarf sample of Pauli et al. (2006). These authors performed a detailed kinematic analysis of 398 DA white dwarfs using the same method as applied here.

the abundance analysis of Blanchette et al. (2008). Note that these are the same models as used by Green et al. (2011) in their analysis, and that the metal abundances used are representative of hot subdwarfs in general, but were not tailored to the extremely peculiar abundance profile of LS IV-14°116. The combined UVES spectrum was analysed using the same models, but this time convolved to the appropriate 0.1 Å wavelength resolution. Here, we combined the blue part of the pipeline-reduced individual spectra as available from the ESO Phase 3 data products archive.

The best-fit synthetic spectra are shown together with the observed FORS2 and UVES spectra and the inferred atmospheric parameters in Fig. 2. While the values inferred are not compatible within the formal errors (which are well known to underestimate the true uncertainties), they both yield a value of $\log g$ close to that inferred by Green et al. (2011). Given the errors almost certainly introduced when combining the echelle orders and fixing the continuum of the UVES spectra, we believe the FORS2 values to be more reliable. Therefore, we adopt $T_{\text{eff}}=35,150$ K and $\log g=5.88$ in what follows. These values place LS IV-14°116 firmly on the He-burning main sequence, as can be seen in Fig. 3.

3.2. Kinematics

We searched the series of archival UVES spectra for RV variations by measuring the Doppler shift of the spectral lines with respect to their rest wavelength. This was achieved by fitting a set of mathematical functions with the FITSB2 routine (Napiwotzki et al. 2004) to the He I lines at 4026.2, 4120.9 and 4387.9 Å. We used a polynomial to match the continuum, while the line wings were fit with a Lorentz profile and the line core with a Gaussian profile. Heliocentric corrections were then applied to the times and velocities.

Averaging the RV measurements from the individual UVES spectra we infer an absolute average radial velocity shift of

$v_r = -149.1 \pm 2.1$ km/s. This is in line with the ~ -150 km/s shift seen in our FORS2 spectra. Note also that the UVES spectra do not show a radial velocity drift comparable to that found for the FORS data, confirming the instrumental nature of that effect. Upon reinspection, the lower spectral resolution ($\Delta\lambda = 9$ Å) Bok telescope spectra used for the spectral analysis of Green et al. (2011) show a compatible wavelength shift. There can then be no doubt that the blueshift detected is real. Since single subdwarf B stars in the Galactic field tend to have significantly lower radial velocities ($|RV| < 40$ km/s, Betsy Green, 2014, private communication) we found this highly intriguing and decided to run a kinematic analysis.

The velocity components of LS IV-14°116 were computed based on its coordinates ($\alpha_{2000} = 20^{\text{h}}57^{\text{m}}38.8^{\text{s}}$, $\delta_{2000} = -14^{\circ}25'47''$ from Simbad), radial velocity (determined from the UVES spectra above), proper motion and distance. All the parameters were varied within the errors adopted. The distance was estimated to be $d = 0.44 \pm 0.04$ kpc following the method described by Ramspeck et al. (2001) and assuming the values of $\log g$ and T_{eff} as inferred from our FORS2 spectra shown in the left panel of Fig. 2 (but increasing the errors to more realistic values of 0.05 and 500 K respectively), a canonical mass of $0.47 M_{\odot}$, a magnitude of $V = 13.03$ from Simbad, and using the extinction maps of Schlafly & Finkbeiner (2011). The proper motion was taken from the PPMXL catalogue via Vizier to be $\mu_{\alpha} \cos \alpha = 8.2 \pm 1.8$ mas/yr and $\mu_{\delta} = -130.6 \pm 1.8$ mas/yr. Since these observed parameters are in the heliocentric reference frame, they need to be supplemented by Solar velocity and position information in order to be transferred to the Galactic rest frame. Here we assumed the distance of the Sun from the Galactic centre to be 8.4 kpc, its motion relative to the Local Standard of Rest (LSR) to have components $v_{x\odot}=11.1$ km/s, $v_{y\odot}=12.24$ km/s, $v_{z\odot}=7.25$ km/s (Schönrich et al. 2010), and the velocity of the LSR to be $V_{\text{LSR}} = 242$ km/s, as predicted by Model I of Irigang et al. (2013).

The position and kinematic properties of LS IV-14°116 were then computed following the equations given in Appendix A. We derived Galactic coordinates $x = -8.10 \pm 0.03$ kpc, $y = 0.20 \pm 0.02$ kpc, $z = -0.25 \pm 0.02$ kpc and a Galactic restframe velocity of 60.39 ± 19.37 km/s, with cartesian velocity components $v_x = -14.66 \pm 7.65$ km/s, $v_y = -55.23 \pm 22.28$ km/s and $v_z = -10.21 \pm 9.84$ km/s. This translates to a Galactic radial velocity component $U = 13.23 \pm 8.28$ km/s and a Galactic rotational velocity component $V = -55.56 \pm 22.13$ km/s. The negative value of V immediately indicates a retrograde orbit, i.e. LS IV-14°116 is orbiting the Galactic centre in the opposite direction to the disk, implying it to be a halo star. Fig. 4 illustrates this quite nicely: while the stars of the reference sample fall mostly within the 3σ contours expected for the thin or thick disk population in the $U - V$ plane, LS IV-14°116 lies well outside these contours. It must therefore be a halo star that by chance is relatively close by. For completeness, it should be noted that using the atmospheric parameters and in particular the lower surface gravity of Naslim et al. (2011) for the distance estimate gives an even lower value of $V \sim -150$ km/s, i.e. the qualitative conclusion that LS IV-14°116 is a halo star does not change.

4. Conclusion

The conclusions we can draw from the study presented here are:

- LS IV-14°116 does not have a strong magnetic field. Formally, the FORS2 spectro-polarimetric measurements exclude a mean longitudinal magnetic field higher than 300 G.
- The atmospheric parameters derived from the combined FORS2 total intensity spectrum are consistent with LS IV-14°116 residing on the Helium main sequence.
- Based on a kinematic analysis, LS IV-14°116 appears to belong to the halo population of our Galaxy.

The fact that LS IV-14°116 does not have a discernable magnetic field means that we need to find alternative scenarios to explain the pulsations as well as the extremely peculiar abundance pattern. One currently popular idea is that LS IV-14°116 is a pre-Helium Main Sequence (pre-He-MS) star that is still in the process of settling onto the Extreme Horizontal Branch. In this scenario, the observed abundance pattern can be qualitatively understood in terms of an atmosphere not yet sorted by diffusion. Diffusion, if unimpeded by other processes, will drain the atmosphere of a hot subdwarf of metals (and even Helium if any Hydrogen is present) on a time-scale of $\lesssim 10^4$ years, negligible compared to the 10^8 -year time-scale of the He-core-burning phase (see, e.g. Fig. 11 of Latour et al. 2014). It is clear that in order for He-rich sDBs to exist in the numbers observed, diffusion must be slowed down, possibly by internal turbulence or a weak stellar wind, however the details are far from being understood.

The pre-He-MS scenario is supported by the qualitative modelling of the pulsations observed in LS IV-14°116 in terms of an ϵ -mechanism acting in the He-burning shells that appear before the star settles in the core He-burning phase (Miller Bertolami et al. 2011). Depending on the exact model parameters used, periods overlapping those observed in LS IV-14°116 can be excited for models in the right temperature range around 35,000 K. However, maximum instability occurs at $\log g \sim 5.2$ -5.7 and pulsations cease for models with $\log g \gtrsim 5.8$ since the ϵ -mechanism is active only during the He-burning subflashes following the primary He-core flash, which stop once the

star settles on the He-MS. According to the atmospheric parameters derived above, LS IV-14°116 resides on the He-MS with $\log g \sim 5.9$.

There are then two options: either LS IV-14°116 has already settled on the He-MS, or our atmospheric parameters are wrong. While we have convincing reasons to believe our atmospheric parameters to be rather accurate for H-sdB stars in the 29,000-36,000 K range thanks to frequent cross-checks with asteroseismic modelling, it is possible that the atmospheric parameters inferred for LS IV-14°116 will change slightly when including metals appropriate for the peculiar abundance profile observed in the model atmospheres. Note however that the assumed metal abundance affects mostly the derived value of T_{eff} and has little impact on $\log g$. A more precise abundance analysis of LS IV-14°116 is currently planned by another group on the basis of UV-spectroscopy scheduled with HST, and will hopefully provide new insights on this.

If LS IV-14°116 is confirmed as a bona fide helium core-burning star, the driving of the pulsations and the unusual surface composition remain an enigma. We believe that the halo membership may be of importance in this context. Indeed, the atmospheric properties of halo and globular cluster hot subdwarfs show systematic differences compared to those in the Galactic disk in terms of their relative distribution in $\log g - T_{\text{eff}}$ space (e.g. Latour et al. 2014; Németh et al. 2012). Moreover, there is first observational evidence that intermediate He-rich stars in general belong to the halo (P. Németh, 2014, private communication). The pulsational properties of hot subdwarfs in some globular clusters and the field also appear to be different. For instance, the rapid sDB pulsators of the field population have not yet been discovered in a globular cluster despite systematic searches (e.g. Randall et al. 2011), and conversely, the fast sdO pulsators recently found in ω Cen do not appear to have counterparts among field sdO stars (Johnson et al. 2014). It is not at all clear why this is the case, but must reflect differences in the internal structure of the stars in question.

Presumably, the metallicity of the subdwarf progenitor population plays an important role. Apart from being metal-poor, the red giant progenitors of sDB stars in the halo are old compared to those in the Galactic disk and have a relatively low mass of around $0.8 M_{\odot}$. The progenitor mass is in turn predicted to influence the core mass of the sDB (Han et al. 2002). It was also suggested that different formation channels for sDB stars dominate depending on the age of the population, the white dwarf merger scenario becoming more important for older populations (Han 2008). Besides updated pulsation models including variable envelope compositions, a better observational characterisation of the different hot subdwarf populations is needed to address these issues. It would be particularly interesting to run kinematic analyses for all well-studied subdwarfs with unusually large absolute radial velocities and/or proper motions to assess whether they are in fact halo or Galactic disk stars. Statistically significant samples for these populations could then be subjected to detailed atmospheric analyses and contrasted with each other. Ultimately, the asteroseismic exploitation of halo sDB pulsators may be used to compare the masses and structural compositions of these stars with those of their Galactic disk counterparts.

Acknowledgements. S.K.R. gratefully acknowledges the help of the Paranal Science Operations, Engineering and Software staff, in particular Linda Schmidtobreick, with the observations. The program used for the kinematic calculations was kindly provided by Andreas Irrgang. We thank Betsy Green for sharing her unpublished radial velocities of hot subdwarfs. Further thanks go to Peter Németh, Marcelo Miller Bertolami, Uli Heber and Marilyn Latour for interesting and insightful discussions, and Pascal Petit, Stéphane Charpinet, and Valérie Van Grootel for their interest and motivation. We also acknowledge the

PI of the archival UVES data, Simon Jeffery. This research has made use of the SIMBAD database, operated at CDS, Strasbourg, France.

References

- Ahmad, A. & Jeffery, C. S. 2005, *A&A*, 437, L51
- Bagnulo, S., Fossati, L., Kochukhov, O., & Landstreet, J. D. 2013, *A&A*, 559, A103
- Bagnulo, S., Landi Degl'Innocenti, E., Landolfi, M., & Leroy, J. L. 1995, *A&A*, 295, 459
- Bagnulo, S., Landstreet, J. D., Fossati, L., & Kochukhov, O. 2012, *A&A*, 538, A129
- Bagnulo, S., Szeifert, T., Wade, G. A., Landstreet, J. D., & Mathys, G. 2002, *A&A*, 389, 191
- Blanchette, J.-P., Chayer, P., Wesemael, F., et al. 2008, *ApJ*, 678, 1329
- Brassard, P., Fontaine, G., Chayer, P., & Green, E. M. 2010, in *American Institute of Physics Conference Series*, Vol. 1273, American Institute of Physics Conference Series, ed. K. Werner & T. Rauch, 259–262
- Brown, T. M., Sweigart, A. V., Lanz, T., Landsman, W. B., & Hubeny, I. 2001, *ApJ*, 562, 368
- Charpinet, S., Fontaine, G., Brassard, P., et al. 1997, *ApJ*, 483, L123+
- Charpinet, S., Fontaine, G., Brassard, P., & Dorman, B. 1996, *ApJ*, 471, L103+
- Charpinet, S., Van Grootel, V., Fontaine, G., et al. 2011, *A&A*, 530, A3
- Clausen, D. & Wade, R. A. 2011, *ApJ*, 733, L42
- D'Antona, F., Bellazzini, M., Caloi, V., et al. 2005, *ApJ*, 631, 868
- Green, E. M., Fontaine, G., Reed, M. D., et al. 2003, *ApJ*, 583, L31
- Green, E. M., Guvenen, B., O'Malley, C. J., et al. 2011, *ApJ*, 734, 59
- Han, Z. 2008, *A&A*, 484, L31
- Han, Z., Podsiadlowski, P., Maxted, P. F. L., & Marsh, T. R. 2003, *MNRAS*, 341, 669
- Han, Z., Podsiadlowski, P., Maxted, P. F. L., Marsh, T. R., & Ivanova, N. 2002, *MNRAS*, 336, 449
- Heber, U., Geier, S., & Gaensicke, B. 2013, in *European Physical Journal Web of Conferences*, Vol. 43, European Physical Journal Web of Conferences, 4002
- Irrgang, A., Wilcox, B., Tucker, E., & Schiefelbein, L. 2013, *A&A*, 549, A137
- Jeffery, C. S. 2012, in *Astronomical Society of the Pacific Conference Series*, Vol. 462, Progress in Solar/Stellar Physics with Helio- and Asteroseismology, ed. H. Shibahashi, M. Takata, & A. E. Lynas-Gray, 47
- Johnson, C., Green, E., Wallace, S., et al. 2014, in *Astronomical Society of the Pacific Conference Series*, Vol. 481, Astronomical Society of the Pacific Conference Series, ed. V. van Grootel, E. Green, G. Fontaine, & S. Charpinet, 153
- Johnson, D. R. H. & Soderblom, D. R. 1987, *AJ*, 93, 864
- Kawka, A. & Vennes, S. 2012, *MNRAS*, 425, 1394
- Kilkenny, D., Koen, C., O'Donoghue, D., & Stobie, R. S. 1997, *MNRAS*, 285, 640
- Landolfi, M., Bagnulo, S., & Landi Degl'Innocenti, M. 1998, *A&A*, 338, 111
- Landstreet, J. D., Bagnulo, S., & Fossati, L. 2014, *A&A*, 572, A113
- Landstreet, J. D., Bagnulo, S., Fossati, L., Jordan, S., & O'Toole, S. J. 2012a, *A&A*, 541, A100
- Landstreet, J. D., Bagnulo, S., Valyavin, G. G., et al. 2012b, *A&A*, 545, A30
- Latour, M., Randall, S. K., Fontaine, G., et al. 2014, *ArXiv e-prints*
- Mathys, G. & Hubrig, S. 2006, *A&A*, 453, 699
- Miller Bertolami, M. M., Corsico, A. H., & Althaus, L. G. 2011, *ApJ*, 741, L3
- Napiwotzki, R., Yungelson, L., Nelemans, G., et al. 2004, in *Astronomical Society of the Pacific Conference Series*, Vol. 318, Spectroscopically and Spatially Resolving the Components of the Close Binary Stars, ed. R. W. Hilditch, H. Hensberge, & K. Pavlovski, 402–410
- Naslim, N., Jeffery, C. S., Behara, N. T., & Hibbert, A. 2011, *MNRAS*, 412, 363
- Németh, P., Kawka, A., & Vennes, S. 2012, *MNRAS*, 427, 2180
- O'Toole, S. J., Jordan, S., Friedrich, S., & Heber, U. 2005, *A&A*, 437, 227
- Pauli, E.-M., Napiwotzki, R., Heber, U., Altmann, M., & Odenkirchen, M. 2006, *A&A*, 447, 173
- Petit, P., Van Grootel, V., Bagnulo, S., et al. 2012, in *Astronomical Society of the Pacific Conference Series*, Vol. 452, Fifth Meeting on Hot Subdwarf Stars and Related Objects, ed. D. Kilkenny, C. S. Jeffery, & C. Koen, 87
- Ramspeck, M., Heber, U., & Edelman, H. 2001, *A&A*, 379, 235
- Randall, S. K., Calamida, A., Fontaine, G., Bono, G., & Brassard, P. 2011, *ApJ*, 737, L27
- Reid, M. J. & Brunthaler, A. 2004, *ApJ*, 616, 872
- Schlafly, E. F. & Finkbeiner, D. P. 2011, *ApJ*, 737, 103
- Schönrich, R., Binney, J., & Dehnen, W. 2010, *MNRAS*, 403, 1829
- Schuh, S., Huber, J., Dreizler, S., et al. 2006, *A&A*, 445, L31
- Van Grootel, V., Charpinet, S., Brassard, P., Fontaine, G., & Green, E. M. 2013, *A&A*, 553, A97

Appendix A: Kinematic calculations

We calculated the kinematic properties of LS IV-14°116 based on the input parameters given in section 3.2 using the equations detailed below. To begin with, the polar coordinates of the target are converted to cartesian coordinates using

$$C = d \cdot \begin{pmatrix} \cos \alpha \cos \delta \\ \sin \alpha \cos \delta \\ \sin \delta \end{pmatrix}$$

where d is the distance of the star (from the Sun) and α and δ are the right ascension and declination respectively. This cartesian coordinate system is then rotated and shifted to x, y, z coordinates in the Galactic coordinate system, defined by the Galactic centre being at (0,0,0), the Sun being at $x = -8.4$ kpc (i.e. its assumed distance from the Galactic centre), and the positive z -axis pointing towards the Galactic North pole, using

$$\begin{pmatrix} x \\ y \\ z \end{pmatrix} = M \cdot C + \begin{pmatrix} -d_{\odot-GC} \\ 0 \\ 0 \end{pmatrix}$$

where $d_{\odot-GC}$ is the distance from the Sun to the Galactic centre and

$$M = \begin{pmatrix} V_{GC}^T \\ V_y^T \\ V_{NGP}^T \end{pmatrix}$$

$$V_{GC} = \begin{pmatrix} \cos \alpha_{GC} \cos \delta_{GC} \\ \sin \alpha_{GC} \cos \delta_{GC} \\ \sin \delta_{GC} \end{pmatrix}$$

$$V_{NGP} = \begin{pmatrix} \cos \alpha_{NGP} \cos \delta_{NGP} \\ \sin \alpha_{NGP} \cos \delta_{NGP} \\ \sin \delta_{NGP} \end{pmatrix}$$

$$V_y = -(V_{GC} \times V_{NGP})$$

are the rotation matrix transformations applied to the x, z, y axes respectively (Johnson & Soderblom 1987). We performed these transformations assuming Galactic Centre coordinates $\alpha_{GC} = 17:45:37.224$, $\delta_{GC} = -28:56:10.23$ and Galactic North Pole coordinates $\alpha_{NGP} = 12:51:26.282$, $\delta_{NGP} = 27:07:42.01$ as determined by Reid & Brunthaler (2004).

For the computation of the velocities, the individual observed velocity components are converted to cartesian coordinates separately and subsequently added to give the total velocity v_C in the cartesian system:

$$v_{rc} = v_r \cdot \begin{pmatrix} \cos \alpha \cos \delta \\ \sin \alpha \cos \delta \\ \sin \delta \end{pmatrix}$$

$$v_{\delta} = \mu_{\delta} \cdot d \cdot \begin{pmatrix} -\cos \alpha \sin \delta \\ -\sin \alpha \sin \delta \\ \cos \delta \end{pmatrix}$$

$$v_{\alpha} = \mu_{\alpha} \cos \delta \cdot d \cdot \begin{pmatrix} -\sin \alpha \\ \cos \alpha \\ 0 \end{pmatrix}$$

$$v_C = v_{rc} + v_\delta + v_\alpha$$

where v_r is the measured radial velocity, μ_δ is the observed proper motion in declination, and $\mu_\alpha \cos \delta$ is the observed proper motion in right ascension. The resulting cartesian velocity components are then transformed into velocity components v_x, v_y, v_z in the Galactic coordinate system with

$$\begin{pmatrix} v_x \\ v_y \\ v_z \end{pmatrix} = M \cdot v_C + \begin{pmatrix} v_{x\odot} \\ v_{y\odot} + v_{lsr} \\ v_{z\odot} \end{pmatrix}$$

where v_{lsr} is the velocity of the Local Standard of Rest and $v_{x\odot}, v_{y\odot}, v_{z\odot}$ are the velocity components of the Sun in the Galactic reference frame. The total Galactic restframe velocity is then given by

$$v_{\text{grf}} = \sqrt{v_x^2 + v_y^2 + v_z^2}$$

The Galactic radial velocity and rotational velocity components of the star are then respectively computed as

$$U = \frac{xv_x + yv_y}{\sqrt{x^2 + y^2}}$$

$$V = -\frac{xv_y - yv_x}{\sqrt{x^2 + y^2}}$$